ACS APPLIED MATERIALS & INTERFACES

Research Article

www.acsami.org

Regulating MC3T3-E1 Cells on Deformable Poly(ε-caprolactone) Honeycomb Films Prepared Using a Surfactant-Free Breath Figure Method in a Water-Miscible Solvent

Xiaohui Wu[†] and Shanfeng Wang*[,†,‡]

[†]Department of Materials Science and Engineering, The University of Tennessee, Knoxville, Tennessee 37996, United States

[‡]Biosciences Division, Oak Ridge National Laboratory, Oak Ridge, Tennessee 37831, United States

ABSTRACT: Honeycomb poly(ε-caprolactone) (PCL) films with tunable pore diameters of 3.5, 6.0, and 10 μm were fabricated directly from solutions in water-miscible, relatively nontoxic tetrahydrofuran using the breath-figure method without assistance of a surfactant. These honeycomb PCL films were characterized in terms of structures and enhanced hydrophobicity. Aiming at fostering bone tissue engineering outcomes, we cultured mouse preosteoblastic MC3T3-E1 cells on these honeycomb films as well as on the flat control, and evaluated their adhesion, spreading, proliferation, alkaline phosphatase (ALP) activity, and calcium content. These cell behaviors were further correlated with the expression levels of integrin subunits of α_1, α_2, β_1, and bone-specific gene markers of ALP, collagen type I (COL I), osteocalcin (OCN), and osteopontin (OPN). Honeycomb PCL films remarkably promoted MC3T3-E1 cell adhesion, spreading, proliferation, differentiation, and gene expression. This effect was more prominent when the pore diameter was smaller in the studied range. In addition, honeycomb PCL films were stretched into groove-like structures, on which MC3T3-E1 cells were aligned with a smaller cell area, a higher percentage of aligned cells, and a higher cell elongation ratio when the pores were smaller.

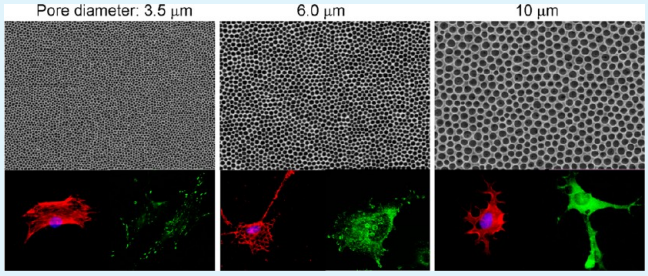

KEYWORDS: *poly(ε-caprolactone), honeycomb films, the breath figure method, scaffolding, MC3T3-E1 cell behavior, bone tissue engineering*

INTRODUCTION

It is a great challenge to repair massive defects in bone when the balance between resorption and regeneration is lost in its degeneration caused by aging and disease.[1,2] A variety of synthetic and natural polymers have been developed as filler materials in bone surgery.[1,2] Although they can handle immediate problems, there exist some prominent disadvantages such as mismatch in mechanical properties and lack of sufficient biocompatibility and bioactivity with the surrounding tissue over long-term observation of implants made from these materials.[1,2] Therefore, much attention has been drawn to developing new-generation biomaterials with improved mechanical properties, biocompatibility, and bioactivity using advanced biomimetic approaches.

One biomimetic approach is to mimic basement membrane, which exists throughout vertebrate body and provides substrata for overlying cellular structures. They are composed of extracellular matrix (ECM) proteins such as fibrous collagen, laminin, and fibronectin, which supply integrin receptors for cell anchorage and regulate subsequent events.[3,4] Structural features at the micro- and nanometer scales, the main topography of basement membranes, and their mechanical properties dramatically affect integrin-cytoskeleton links and cell functions.[3−5] To mimic these complex features, synthetic substrates with grooves, pits, pores, wells and nodes, spheres, or ridges, have been developed.[3,4,6−8] Many methods such as phase separation, colloidal templating, and lithography have been used to fabricate porous topography with ordered structures.[3,4] Among these methods, the breath-figure method is very simple and economical, in which polymer is dissolved in in a volatile and water-immiscible solvent such as chloroform ($CHCl_3$), benzene, and carbon disulfide (CS_2) and then the solution evaporates quickly in a humid environment.[9,10] The sharp drop of the temperature in polymer solution upon rapid solvent evaporation causes condensation of water vapor in air. Subsequently polymer precipitates and stabilizes water droplets with identical diameters orderly packed in a hexagonal array on the solution/air interface as the result of capillary force and convection currents. Then honeycomb polymer films can be obtained after complete drying.

Poly(ε-caprolactone) (PCL) is a biodegradable semicrystalline polymer with excellent biocompatibility and biodegradability for biomedical applications and has been fabricated into porous bone tissue engineering scaffolds using different methods.[11] Honeycomb PCL films were prepared using water-immiscible solvents with the assistance of amphiphilic

Received: July 15, 2012
Accepted: August 13, 2012
Published: August 13, 2012

copolymers such as cocarboxyhexyl acrylamide.[12−20] PCL films with multilayers of ordered pores were also prepared using silica microspheres as the template.[21] Honeycomb PCL films with different micropore diameters were further used to regulate adhesion, spreading, and proliferation of endothelial cells, hepatocytes, epidermal keratinocytes, and dermal fibroblasts, and differentiation of neural stem cells.[8,14−20] There lack studies on regulating osteoblastic adhesion, differentiation, and gene expression on honeycomb films of biodegradable polymers with tunable micropores, although porous substrates/scaffolds have been developed for enhancing bone cell functions.[22,23] In addition, this study was the first time to prepare honeycomb PCL films from solutions in water-miscible tetrahydrofuran (THF) via the breath-figure method without the need of a surfactant. Previously THF was also used as a solvent for poly(L-lactide), poly(methyl methacrylate), cellulose acetate-butyrate, and carboxylate-terminated polystyrene to prepare porous films and fibers.[24−27] Compared with toxic $CHCl_3$ and benzene used in the previous preparation of honeycomb PCL films,[12−20] THF is apparently advantageous because it is relatively nontoxic.

In this report, we first present fabrication and characterization of the honeycomb PCL films with tunable pores. Then we discuss the evaluation of these honeycomb films as bone tissue engineering substrates by culturing mouse preosteoblastic MC3T3-E1 cells on them and the flat control. Cell adhesion, spreading, proliferation, alkaline phosphatase (ALP) activity, and calcium content were determined and correlated with gene expression of four bone-specific differentiation markers, ALP, collagen type I (COL I), osteocalcin (OCN), and osteopontin (OPN). Honeycomb PCL films were further stretched into groove-like structures, on which MC3T3-E1 cells were cultured for evaluating cell alignment. This study not only supplies a convenient method to produce large-area porous substrates for biomedical applications, but also demonstrates an appropriate range of micropore dimensions for enhancing preosteoblastic cell functions.

EXPERIMENTAL SECTION

Fabrication of PCL Films. PCL (M_n = 97 700 g mol^{-1}, M_w = 144 200 g mol^{-1}) used in this study was purchased from Aldrich (Milwaukee, WI) and used in our previous studies.[28−30] PCL was dissolved in distilled THF (Aldrich) at a concentration of 50 mg mL^{-1}. The PCL solution was then cast onto clean glass slides and put in a chamber. At a relative humidity of 75%, honeycomb films with pore diameters of 3.5, 6.0, and 10 μm were fabricated by controlling the airflow rate at 100, 50, and 0 mL min^{-1}, respectively. The PCL films became opaque gradually and evaporation was conducted for 5 min prior to further treatment. For comparison, flat films were also prepared by casting the same PCL solution onto clean glass slides without a humid environment. Stretched PCL films were prepared by stretching all the films at an elongation ratio, i.e., the ratio of the final length to the initial length, of 4.5 at room temperature (~20 °C).

Surface Topography. The as-prepared PCL films were fixed on glass slides, dried completely in vacuum, and sputter-coated with a gold−palladium layer (Emscope SC 500, Elexience). The surface morphology of the honeycomb films was observed using Scanning Electron Microscopy (SEM; S-3500, Hitachi Instruments, Tokyo, Japan) at an accelerating voltage of 5 kV.

Water Contact Angle and Protein Adsorption. PCL films were dried completely in vacuum overnight before the measurements. Water contact angles were determined using a Ramé-Hart NRC C. A. goniometer (model 100−00−230) and water droplets were photographed using 3.0 megapixel camera (Moticam 2300, Motic) at room temperature. To evaluate serum protein adsorption, we soaked flat and honeycomb PCL films for 4 h at 37 °C in the media used for culturing MC3T3-E1 cells. The films were rinsed with PBS five times to remove unattached proteins, and immersed in 300 μL of 1% sodium dodecyl sulfate (SDS) solution five times with 1 h interval to collect proteins adsorbed on the films. A MicroBCA protein assay kit (Pierce, Rockford, IL) and a microplate reader (SpectraMax Plus 384, Molecular Devices, Sunnyvale, CA) were used to determine the concentrations of the proteins in the collected SDS solutions. All data was calibrated using a standard curve constructed from albumin solutions according to the manufacturer's instruction.

Cell Culture. Mouse MC3T3-E1 cells (ATCC, Manassas, VA) were cultured in the same way as reported by us.[28−34] Prior to cell studies, all PCL films were immersed in 70% alcohol solution overnight to remove the residues from sample preparation, further sterilized by 70% alcohol solution for 3 × 30 min, and dried in vacuum. Cells were seeded on the samples at a density of ~15,000 cells/cm^2 in α-Minimum Essential Media (α-MEM, Gibco) containing 10% fetal bovine serum (FBS, Gibco) and 1% penicillin/streptomycin (Gibco). Then the cells were cultured for 4 h and 1, 2, and 4 days in an incubator at 37 °C with humidity of 95% and 5% CO_2.

Immunofluorescence Microscopy and Cell Morphology. MC3T3-E1 cells on the films were fixed with 16% paraformaldehyde (PFA) solution for 30 min. After PFA was removed, cells were rinsed with phosphate buffered saline (PBS) twice and permeabilized with 0.2% (v/v) Triton X-100. Then the cells were washed with PBS and stained with rhodamine-phalloidin (RP) for 2 h at 37 °C, followed by 4′,6-diamidino-2-phenylindole (DAPI) staining at room temperature. An Axiovert 25 light microscope (Carl Zeiss, Germany) was used for photographing. Cells were counted using DAPI-stained images and the mean number of nuclei per field (n = 20) was calculated. Average cell area was measured from 20 nonoverlapping cells at day 1 using ImageJ software (National Institutes of Health, Bethesda, MD). F-actin cytoskeleton at day 1 was observed using a confocal microscope (SP2, Leica). Focal adhesions (FAs) of cells were stained with mouse monoclonal antivinculin antibody (V9264, Sigma-Aldrich) for 1 h at 37 °C followed by five rinses with PBS. Then the FAs were labeled by antimouse IgG-FITC antibody (F0257, Sigma) at 37 °C for 5 h and were recorded under a confocal microscope. For SEM imaging, cells cultured for 1 day were fixed in 5% paraformaldehyde (w/v) for 30 min and rinsed with PBS for three times. Then all samples were dehydrated with gradient ethanol solutions (30, 50, 70, 95, and 100%) for 20 min twice at each concentration and dried in vacuum overnight. After being sputter-coated with one gold−palladium layer, the samples were observed using SEM in the same way for characterizing polymer film topography.

Characterization of Aligned Cells. MC3T3-E1 cells cultured on the stretched PCL films were fixed, stained, photographed, and analyzed using ImageJ as described above. An ellipse was used to approximate the cell shape and cell elongation was quantified using the extent of the ellipse deformation, which was the ratio of the difference between the long-axis length and short-axis length to the short-axis length. Cells were considered as aligned when the angle between the long axis of the approximated ellipse and the direction of the underlying polymer microgroove structure was smaller than 15°. The percentage of cell alignment was calculated by dividing the number of aligned cells by the entire cell number. For each sample, 200 cells were analyzed to determine these two parameters. Average cell area was also measured from 30 cells in the fluorescent images.

ALP Activity and Calcium Content. After 14 days of cell culture, all PCL films were transferred to new plastic tubes and rinsed with PBS twice to remove unattached cells. Then the adherent cells were collected by trypsinization, which was terminated by adding α-MEM. The cell suspension was centrifuged for 4 min at 1000 rpm, rinsed with PBS, and then centrifuged again for 4 min at 1000 rpm. The obtained cell pellet was suspended in 1 mL of 0.2% Nonidet P-40 solution and sonicated in ice water for 2 min. A fluorescence-based ALP detection kit (Sigma, St. Louis, MO) and a QuantiChrom calcium assay kit (BioAssay Systems, Hayward, CA) were used to determine the ALP activity and calcium content of the cell lysate, respectively.[32]

Gene Expression. For determining the expression levels of integrin α_1, α_2, and β_1, MC3T3-E1 cells were cultured on PCL films for one day. Then the cellular RNA was isolated from the cells using an RNeasy Mini Kit (Qiagen, Valencia, CA) and cDNA was synthesized using a cDNA synthesis kit (Thermo Scientific). Expression of integrin subunits of α_1, α_2, β_1, and glyceraldehyde-3-phosphate dehydrogenase (GAPDH) utilized for normalization of the differences in the amount of total RNA was quantified through real-time polymerase chain reaction (PCR) with a Power SYBR Green PCR Master Mix (Applied Biosystems, Carlsbad, CA) and performed on a thermal cycler with fluorescence detection systems (PTC-200, MJ Research). Expression of ALP, COL I, OCN and OPN was performed after cells were cultured on PCL films for 14 days using the same protocol as described above. All the primers for real-time PCR are shown in Table 1.

Table 1. Oligonucleotide Primer Sequences for Real-Time PCR

gene	primer sequence (5′-3′; F: forward; R: reverse)
COL I	F: TCTCCACTCTTCTAGTTCCT
	R: TTGGGTCATTTCCACATGC
OCN	F: CAAGTCCCACACAGCAGCTT
	R: AAAGCCGAGCTGCCAGAGTT
ALP	F: GCCCTCTCCAAGACATATA
	R: CCATGATCACGTCGATATCC
OPN	F: ACACTTTCACTCCAATCGTCC
	R: TGCCCTTTCCGTTGTTGTCC
Integrin α_1	F: TGAGCCCACCAAGATGAACGA
	R: CCTGGCCGGTGTGATTGT
Integrin α_2	F: ACAAGGCAACTGGCTACTGGT
	R: ACAGGTGGCAGTGGGTAGG
Integrin β_1	F: GGTGTCGTGTTTGTGAATGC
	R: TCCTGTGCACACGTGTCTT
GAPDH	F: ACTTTGTCAAGCTCATTTCC
	R: TGCAGCGAACTTTATTGATG

Statistical Analysis. Protein adsorption and in vitro cell studies were performed in quadruplicates for each group and each time point. The values were expressed as mean ± standard deviation. The statistical significance ($p < 0.05$ or 0.01) in the differences between groups was analyzed by the student's *t*-test.

RESULTS AND DISCUSSION

Morphology and Hydrophilicity of the Honeycomb Films. In the breath-figure method, parameters used to achieve different pore diameters and morphologies include solvent type, air flow rate, humidity, additives, interfacial activity of polymers, and the concentration and amount of polymer solution.[9,10] In this study, the airflow rate was the key factor to regulate the pore diameter of the honeycomb films. When airflow rates of 100, 50, and 0 mL/min were applied in forming honeycomb PCL films, the as-formed average pore diameters were 3.5, 6.0, and 10 μm, respectively (Figure 1A). Faster airflow could accelerate the evaporation process and more efficiently decreased the temperature on the polymer solution, condensing a larger amount of water droplets. Although water and THF are miscible, PCL solution in THF could stabilize water droplets during THF evaporation. Owing to the fast evaporation of the solvent, coalescence of water droplets rarely occurred and thus smaller pores on the surface of polymer solution could be formed at a higher airflow rate. Consistent with other honeycomb films prepared from THF solutions, the honeycomb PCL films here also showed a monolayer architecture with a solid bottom although THF is lighter than water.[24,25] As demonstrated in the inset tilted SEM image for 6.0 μm pores, many pores in the honeycomb films were interconnected when the pore diameter was 6.0 or 3.5 μm, similar to honeycomb PCL films prepared with assistance of an amphiphilic copolymer.[12,15,18,20] Figure 1B shows that the distribution of pore diameter was narrow on all the honeycomb films and the

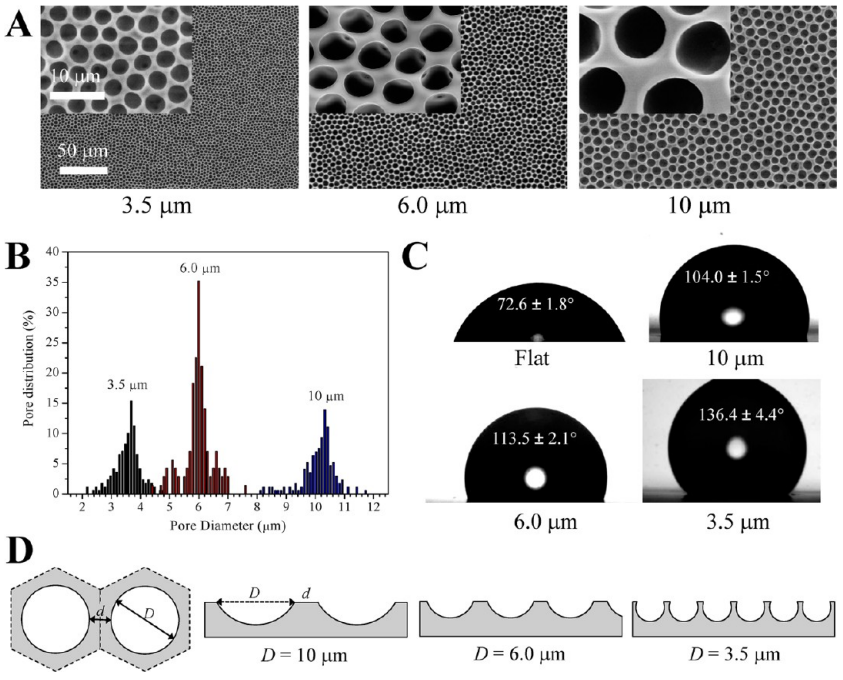

Figure 1. (A) SEM images of the honeycomb films with different pore diameters. Scale bar of 50 μm is applicable for the images with the lower magnification (700×). Scale bar of 10 μm is applicable for the insets (magnification: 5000×). (B) Distribution of pore diameter in the honeycomb films. (C) Micrographs of water droplets and contact angles on the flat and honeycomb films. (D) Model of two adjacent hexagonal unit cells containing pores of diameter D and rim size d (left) and schematic cross-sections of honeycomb films with three different pore diameters.

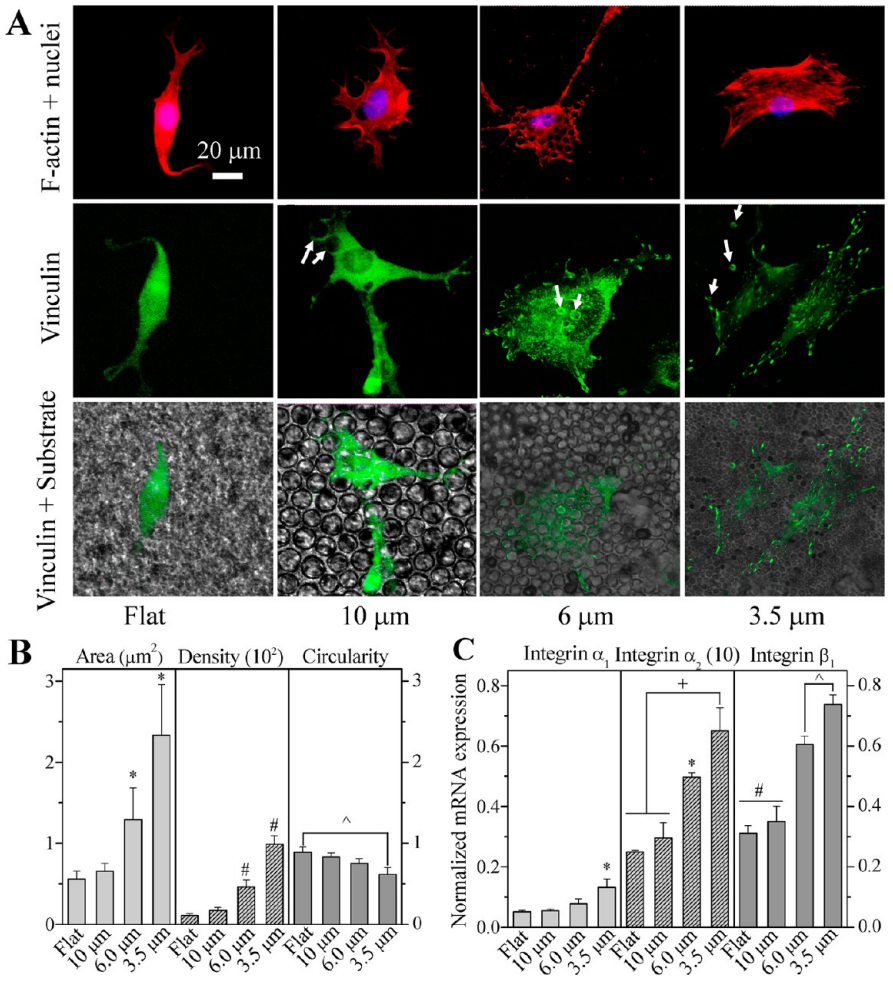

Figure 2. (A) Fluorescent images of MC3T3-E1 cells stained with RP (red) and DAPI (blue) (top row), vinculin-stained cell images (middle row) with arrow heads indicating pores of the honeycomb films, and merged images with the underlying substrates at day 1 postseeding. Scale bar of 20 μm is applicable for all. (B) Area, density, and circularity of FAs. (C) Integrin expression of cells. *, $p < 0.05$; #, $p < 0.01$ relative to others; +, $p < 0.01$;^, $p < 0.05$.

6.0 μm pores were more uniform than the other two. Differential scanning calorimetric tests were performed for the flat and honeycomb PCL films but no differences were found in their melting points and crystallinities, suggesting that formation of the honeycomb pattern on PCL films did not influence the thermal properties.

The wettability of polymer films can be influenced by surface topography.[35−37] As demonstrated in Figure 1C, the water contact angles were 72.6 ± 1.8, 104.0 ± 1.5, 113.5 ± 2.1, and 136.4 ± 4.4° on the flat film and honeycomb films with pore diameters of 10, 6.0, and 3.5 μm, respectively. Micro- or nanostructured surface such as these honeycomb films are known to be more hydrophobic by producing air pockets between substrate surface and water droplets when water droplets were much larger than the dimension of the structures present on substrate surface. The Cassie and Baxter model in eq 1 was employed to predict the water contact angles (θ) on these honeycomb films.[21,35−37]

$$\cos\theta = (1 - f_o)\cos\theta_s + f_o\cos\theta_o \quad (1)$$

where f_o is the fractional flat geometrical area of liquid−air interface beneath a water droplet, θ_s is the water contact angle on the smooth PCL surface, i.e., 72.6° here, and θ_o is the water contact angle on the pore filled with air, which is 180°. When the pore diameters (D) were 10, 6.0, and 3.5 μm, the rim sizes (d) measured from the SEM images in Figure 1A were 3.05 ± 0.25, 1.71 ± 0.40, and 0.83 ± 0.04 μm, and then the f_o values were calculated to be 0.528, 0.553, and 0.592, respectively. They were consistent with the values of 0.532, 0.549, and 0.592 estimated from a hexagonal unit cell model with a pore in the center (Figure 1D).

The water contact angles calculated from eq 1 were 112.6, 114.6, and 117.9° for the honeycomb films with pore diameters of 10, 6.0, and 3.5 μm, respectively. The prediction was higher than the experimental value for 10 μm pores but lower for 3.5 μm pores. Although the model did not predict the strong dependence of water contact angle on the pore diameter, it still provided reasonable explanation for the increased hydrophobicity on the smaller pores. In another study, the water contact angles were 105.6, 104.3, 107.2, and 105.0° on honeycomb PCL films with pore diameters of 5.3, 9.1, 11.8, and 15.6 μm, and rim sizes of 1.8, 3.1, 3.6, and 7.1 μm, respectively.[18] The water contact angle on the flat PCL reported in that study was 74°,[18] close to the θ_o value of 72.6° in the present work. Using these parameters and the model in Figure 1D, we obtained f_o values of 0.505, 0.504, 0.532, and 0.428, in agreement with the porosity data of 0.506, 0.510, 0.547, and 0.426 given in that report.[18] Then we calculated

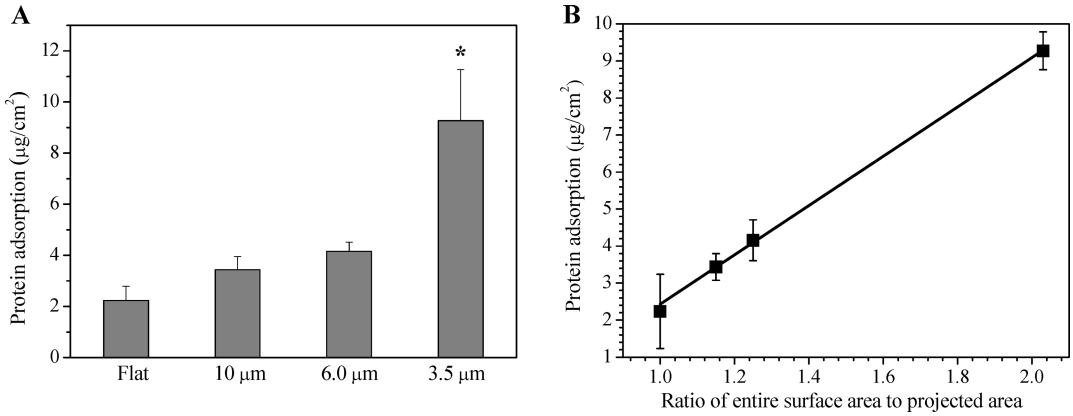

Figure 3. (A) Serum protein adsorption of the flat film and honeycomb films with different pore diameters in α-MEM. *, $p < 0.05$ relative to others. (B) Protein adsorption vs ratio of entire surface area of the films to projected area.

water contact angles of 105.7, 113.8, 111.6, and 111.7° from eq 1. The comparison between these two studies shows that the hydrophobicity of honeycomb PCL films could be significantly strengthened by smaller pores, which can be stronger than the prediction by the Cassie and Baxter model. In addition, the preparation method here of not using an amphiphilic copolymer could also influence the hydrophilicity of the obtained honeycomb films.

Cell Adhesion. After 1-day culture, MC3T3-E1 cell adhesion was examined using fluorescent cell images, characterization of FAs, which are the closest contacts between cells and the underlying substrate, and integrin expression.[38,39] As shown in Figure 2A, all the pores here were subcellular and cells could spread over multiple pores without being aligned along the rim, which was found for cardiac myocytes on overcellular honeycomb PCL films with a pore diameter of 12.5 μm and a rim size of 8.0 μm.[19] Cytoskeleton with F-actin stained red on the flat films had very few stress fibers while the cells on the honeycomb films spread better and had more better-defined stress fibers and protrusions. The cytoskeleton on the honeycomb films with pore diameters of 10 and 6.0 μm was trapped inside the pores. Cells on the honeycomb films with 3.5 μm pores had even better defined stress fibers while no trapped cytoplasm was found. In a previous report, fibroblasts were found to be sensitive to changes in radius of curvature on quartz surface with microscale round pits to decide they chose to enter the pits or move around this obstacle.[40] In this study, larger pores had larger radius of curvature for both pore edge and inside pores, and consequently less sharp discontinuous region between flat-tops and pores, as illustrated in Figure 1D. This may be the reason for MC3T3-E1 cells being trapped by the larger pores.

Vinculin-stained cell images in Figure 2A showed significantly more punctate FAs on the honeycomb films, especially when the pores were smaller, in contrast to diffusive vinculin staining on the flat ones. Moreover, the FAs of MC3T3-E1 cells on the honeycomb films were distributed not only on cell periphery but also along the pore edge. As demonstrated in Figure 2B, FAs were quantified by using the average area of FAs, FA density, i.e., the average number of FAs per cell, and the circularity of FAs, defined as $4\pi \times \text{area/perimeter}^2$. The first two parameters of FAs on the honeycomb films were markedly larger than those on the flat ones and were further strengthened by decreasing the pore diameter. The circularity of FAs on the flat films was close to 1, a measure for a perfect circle. It was lower on the honeycomb films and further decreased when the pore diameter decreased, indicating that the alignment of FAs expressed as the inverse of circularity was enhanced.

Cells react to micro/nanotopography mainly through the "contact guidance" effect.[3−8] For example, FAs of fibroblasts were found to appear on the ridges of microgrooved substrates in an oriented manner and the actin filaments would originate from these adhesion points.[6,41] After FA are aligned, actin filaments or stress fibers in attached cells can also be aligned.[6,7,38,39] Previous findings also suggested that moving or extending cells prefer to be localized at the region of junction or discontinuity,[42] which was the pore edges on the honeycomb films studied here. On the basis of f_o and D, the number of pores and the total length of pore edges in a unit projected area of 1 cm^2 can be estimated. The former parameter increased from 6.8×10^5 to 1.9×10^6 and 6.2×10^6 and the latter increased from 21.3 to 36.6 and 67.7 m when the pore size decreased from 10 to 6.0 and 3.0 μm, respectively. Thus the honeycomb films with small pores generating a large region of junction or discontinuity provide excellent circumstance for cell adhesion and growth.

The FA-ECM interactions involve integrins, which are transmembrane heterodimers of the α-subunit and β-subunit.[5,43,44] Integrins bind different ECM proteins with the external end and cytoskeleton via adapter proteins such as talin, α-actinin, filamin and vinculin, and FAs are based on this integrin-adapter protein−cytoskeleton complex.[5,43,44] ECM proteins, to which osteoblasts can directly react, include fibronectin, COL I, and vitronectin.[43,44] Osteoblasts anchor on substrate surface via integrin receptors which are involved in processes named as "outside-in-signaling" and "inside-out-signaling" between the ECM and the cell. These integrin-involved pathways can regulate subsequent cell adhesion, migration, proliferation, and differentiation. Osteoblasts can express integrin subunits α_1, α_2, α_3, α_4, α_5, α_6, α_v, β_1, β_2, and β_5.[43,45] As shown in Figure 2C, the expression levels of integrin subunits α_1, α_2, and β_1 on the honeycomb films with smaller pores were significantly higher. Binding of $\alpha_1\beta_1$ and $\alpha_2\beta_1$ to type-I collagen, the most abundant bone matrix protein, is critical in regulating osetoblastic differentiation, whereas subunit β_1 is responsible for attachment to fibronectin or COL I.[43−45]

Protein Adsorption. Cell adhesion to a substrate is closely related to proteins adsorbed on the surface, which is dependent on material chemistry and morphology.[5] When the pore

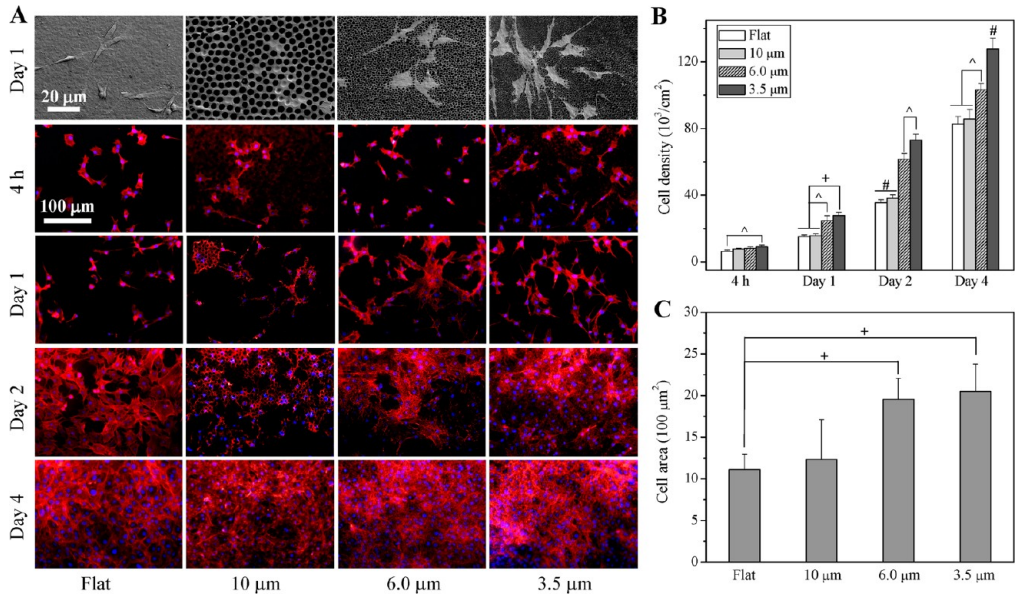

Figure 4. (A) SEM images of MC3T3-E1 cells at day 1 (top row) and fluorescent images of cells stained with RP (red) and DAPI (blue) at 4 h, days 1, 2, and 4 on the flat film and honeycomb films with different pore diameters. Scale bar of 20 μm is applicable to all SEM images and scale bar of 100 μm is applicable to all fluorescent images. (B) Cell proliferation on the films represented by the cell numbers at 4 h, days 1, 2, and 4. (C) Cell area on the films at day 1. *, $p < 0.05$; #, $p < 0.01$ relative to others; +, $p < 0.01$; ^, $p < 0.05$.

diameter in the honeycomb films decreased, the pore edge or the rim also decreased while the entire surface area that included both the flat-tops and inside the pores significantly increased. Figure 1D shows three schematic cross sections of the honeycomb films, in which spherical caps were used to represent the pores left by the water droplets. Using simple geometrical computation, we obtained the entire surface area based on the pore diameters and the heights of spherical caps, which were 2.37, 2.32, and 2.96 μm calculated from the schemes in Figure 1D for pore diameters of 3.5, 6.0, and 10 μm, respectively. When the pore diameter was 10 or 6.0 μm, the spherical cap was smaller than a hemisphere. For 3.5 μm pores, the spherical cap was greater than a hemisphere. The ratios (R_s) of the entire surface area to the projected area were 1.00, 1.15 ± 0.11, and 1.25 ± 0.10, and 2.03 ± 0.18 for the flat films and honeycomb ones with pore diameters of 10, 6.0, and 3.5 μm, respectively. Per a unit projected area, the flat-top area of the honeycomb films, calculated using $(1 - f_o)$, decreased from 0.472 to 0.447 and 0.408, whereas the area inside the pores, calculated using $(R_s + f_o - 1)$, increased from 0.678 to 0.803 and 1.622 when the pore diameter decreased from 10 to 6.0 and 3.5 μm, respectively.

As a result, honeycomb films with larger contract area with the serum proteins in the culture media could promote protein adsorption and it was even higher when pores were smaller. Figure 3A indicates that the concentration of the serum proteins adsorbed on the films increased significantly from 2.24 ± 1.00 μg cm^{-2} for the flat one to 9.27 ± 0.51 μg cm^{-2} for the honeycomb films with the pore diameter of 3.5 μm. As shown in Figure 3B, protein adsorption followed a linear relationship (R^2 = 0.9984) with the ratio of the entire surface area to the projected area, suggesting that it was solely determined by the surface area while the film chemistry did not exert extra effect on the protein adsorption. Although surfaces became more hydrophobic macroscopically, this effect was induced topographically and might not function at the scale of protein size or further influence cell behavior because all the films were rinsed in culture media prior to cell seeding.

MC3T3-E1 cells could sensitively respond to the proteins distributed on the substrates and produce integrin proteins accelerating the formation of FAs and fostering the expression of integrin subunits of α_1, α_2, and β_1 corresponding to osteoblasts, as discussed earlier. However, MC3T3-E1 cells did not spread into most pores, especially when the pore diameter was 3.5 μm, meaning that the proteins adsorbed inside the pores might not contribute much to supporting cell adhesion. In another report, fibroblasts were also seen very occasionally to touch the bottom of the 2 μm grooves while FAs were observed on the wider microgrooves.[41] Assuming that the capability of adsorbing proteins was identical on the surfaces of the flat-tops and inside the pores, we found that the protein concentration on the flat-top area of the honeycomb films with smaller pores would be actually lower. Thus purely the concentration of adsorbed proteins may not be used to interpret the better MC3T3-E1 cell adhesion on the honeycomb films with smaller pores. It should be noted that honeycomb structures could not only enhance protein adsorption but also influence distribution of adsorbed proteins. For example, the fibril-like aggregates of fibronectin were found to locate on the periphery of the pores of honeycomb PCL films, which may further determine the FAs of the cells around these pores.[15−18,20] It is unclear if that was the case in this study but the pore edge itself should be able to stimulate the formation of FAs and then guide and align them, as discussed earlier.

Cell Attachment, Proliferation, and Nuclear Deformation. MC3T3-E1 cell attachment at 4 h and proliferation over 4 days was studied using SEM and fluorescent images (Figure 4A). Better cell adhesion on the honeycomb films with smaller pores as discussed earlier ensured that other adhesion-mediated cell behavior such as cell proliferation, differentiation, and gene expression should also be better.[44] It can be observed from the SEM images that cells could spread and flatten better on the

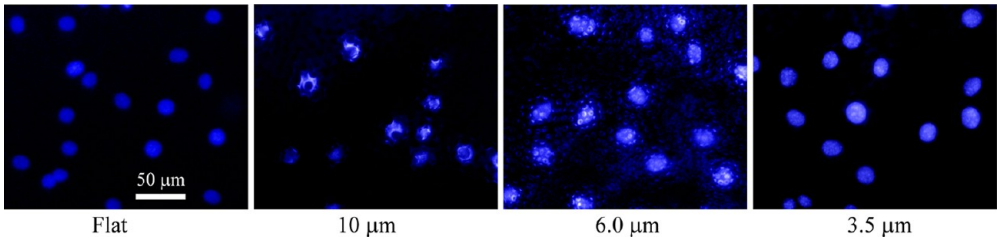

Figure 5. MC3T3-E1 cell nuclei stained with DAPI at day 2 postseeding on the flat film and honeycomb films with different pore diameters.

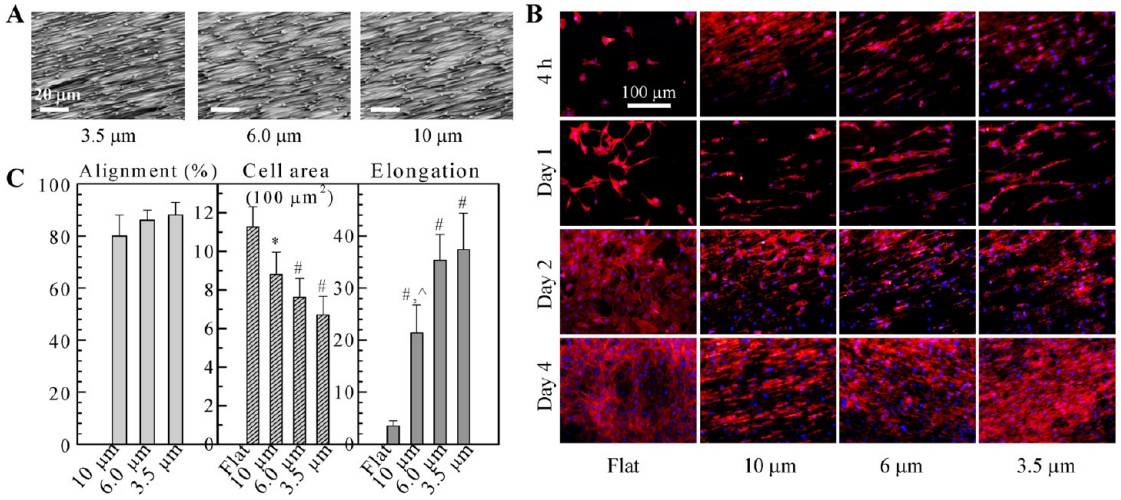

Figure 6. (A) SEM images of the stretched honeycomb films with different pore diameters. Scale bar of 20 μm is applicable to all SEM images (magnification: 1500×). (B) Fluorescent images of MC3T3-E1 cells stained with RP (red) and DAPI (blue) at 4 h, days 1, 2, and 4 on the stretched films. Scale bar of 100 μm is applicable to all fluorescent images. (C) Percentage of cell alignment, cell area, and cell elongation on the stretched films at day 1. *, $p < 0.05$; #, $p < 0.01$ relative to the flat film;^, $p < 0.05$ relative to films with smaller pores.

honeycomb films with pore diameters of 3.5 and 6.0 μm than on the flat films. The cytoplasm on the honeycomb films with a pore diameter of 10 μm was partially or completely trapped inside the pores. The honeycomb films with pore diameters of 3.5 and 6.0 μm, especially for the smaller one, had more cells compared with the flat film and the honeycomb film with pore diameter of 10 μm. This result was further confirmed by the fluorescent images, which showed that cell density increased with the culture time and cells reached confluence at day 4. At days 1 and 2, cytoplasm was clearly trapped and deformed on 10 and 6 μm pores. Cell numbers counted from nuclei stained with DAPI in Figure 4B also demonstrated that cell proliferation was greatly enhanced on the honeycomb films with pore diameters of 6.0 and 3.5 μm, especially the smaller one. Figure 4C shows the average cell area on films, suggesting that cells on films with diameters of 3.5 and 6.0 μm spread and flattened significantly better than those on the flat films.

The effect of pore size in porous substrates on cell behavior has been studied using different materials.[16,19,23,46,47] On honeycomb PCL films with pore diameters of 3−20 μm, keratinocytes and fibroblasts were found to prefer the smallest pores (3−5 μm) in terms of adhesion and proliferation.[16] Smaller pores in this range generated a lager surface area and a longer pore edge whereas overcellular pores could separate cells from communicating with each other, which is detrimental to cell proliferation, signaling, and survival.[16] When the pore diameter was smaller than 1 μm (100−500 nm), MC3T3-E1 cells seeded on porous silica films were elongated on the narrow rims with a much smaller cell area and slower proliferation.[23] When the pore diameter was even smaller (15−100 nm), surface topography at 15 nm could best support mesenchymal stem cell adhesion, proliferation, migration, and differentiation on TiO_2 nanotube surfaces, as this spacing seems optimal for integrin assembly into FAs.[46,47]

MC3T3-E1 cell nuclei stained with DAPI were further analyzed in terms of shape and area, which can be related to gene expression and protein synthesis.[48] As shown in Figure 5, cell nuclei became larger on the honeycomb films and were evidently distorted on the 6.0 and 10 μm pores when cytoplasm was trapped inside the pores. Cell nuclear area at day 2 increased from 235 ± 42 μm^2 on the flat films to 294 ± 79 and 367 ± 52 μm^2 on the honeycomb films with pore diameters of 3.5 and 6.0 μm, respectively. Then it decreased to 326 ± 61 μm^2 when the pore diameter was 10 μm. Cell nuclear deformation may induce difference expression of bone-specific gene markers. For example, MC3T3-E1 cell nuclei were found to be aligned in microgrooved substrates of cross-linked PCL triacrylate (PCLTA) with groove width of 7.5 μm and this nuclear alignment was believed to contribute to higher mineralization and OCN expression.[29] As found previously, upregulated OCN expression from constraining primary rat bone cell nuclei, whereas collagen I synthesis reached maximum at an intermediate value of nuclear distension.[48] The nuclei of human osteosarcoma-derived cells (SaOs-2) were found to be severely deformed on micropillars but it had little effect on its viability, proliferation, and ALP activity.[49] It is still unclear if nuclear expansion found here instead of nuclear alignment and distension could result in high MC3T3-E1 differentiation and gene expression.

Cell Behavior on the Stretched Films. Stretched honeycomb PCL films were characterized using SEM and their microgroove-like topography had a notable effect on MC3T3-E1 cells. As shown in Figure 6A, after deformation of pores, the surface topography presented majorly elongated hexagons, rectangles, and other irregular structures aligned side by side, which was also observed in another set of stretched microporous PCL films.[50] Defects in the honeycomb structure had a remarkable impact on the evolution of pore size and shape during stretching. Overall, the stretched honeycomb films could be considered as microgrooved ones with groove widths of ca. 12, 8, and 5 μm for pore diameters of 10, 6.0, and 3.5 μm, respectively. The groove length and width could be roughly calculated by assuming the pores were perfect circles with uniform dimensions. When the pores were stretched at a stretching ratio of 4.5 along one direction, each groove had a length of 4.5 times as much as the pore diameter. Thus the groove lengths were estimated to be 45, 27, and 15.75 μm for pore diameters of 10, 6.0, and 3.5 μm, in agreement with the values of 40.9 ± 10.3, 30.7 ± 5.2, and 12.6 ± 3.5 μm determined from the SEM images in Figure 6A, respectively. For the rim size or the ridge width, it also increased 4.5 times along the stretching direction but it decreased along the transverse direction. The groove depth should be similar to or lower than the height of spherical cap (2−3 μm) in Figure 1D.

Figure 6B shows the fluorescent images of MC3T3-E1 cells after culture for 4 h, 1, 2, and 4 days on the stretched flat and honeycomb films. The cell densities on the stretched films were almost equal to those on their unstretched counterparts in Figure 4A, B, consistent with our previous finding on microgrooved substrates of cross-linked PCLTA with different groove dimensions.[33] Cell filaments were aligned on the stretched honeycomb films with different groove widths, similar to a previous report when cardiac myocytes were cultured on stretched microporous PCL films.[50] On microgrooved substrates, cells sense forces and adjust shape to obtain optional force equilibrium, inducing aligned cell filaments.[51]

Cell alignment was quantified using three parameters: percentage of alignment, cell area, and cell elongation, as shown in Figure 6C. More than 80% of the cells were aligned on the stretched honeycomb substrates with an increase when the pore diameter or groove width decreased. Cell area on the stretched flat films did not differ from that on the unstretched ones. But it decreased sharply on the stretched honeycomb films and it was smaller when the groove/ridge width was lower. This trend was opposite to the results on the unstretched honeycomb films in Figure 4C. Cell elongation on the stretched flat films was not observed, in contrast to much higher elongation values on the stretched honeycomb films, especially when the pore diameter or groove width was smaller. Our present results agreed with the conclusions in literature that cell alignment often decreases with increasing groove/ridge width or decreasing the groove depth.[4,6,33] Alignment of cell filaments can also induce nuclear elongation because nuclei are mechanically integrated with the entire cell body and intermediate filaments can transfer the forces sensed by cell filaments to the nucleus via mechanotransduction.[6,7,52,53] However, nuclear elongation on the stretched honeycomb films was not observed here, even though they had strong alignment of cell filaments. In a previous report, NIH3T3 fibroblasts proliferated better on a less stiff biaxially stretched PCL membrane with a lower thickness.[54] No difference was found in this study in cell behavior between the flat PCL films before and after stretching, as their thermal and mechanical properties remained the same.

Mineralization and Gene Expression. The honeycomb films not only promoted MC3T3-E1 cell adhesion, spreading, and proliferation, but also enhanced the mineralization process of these cells. As shown in Figure 7, the calcium content and

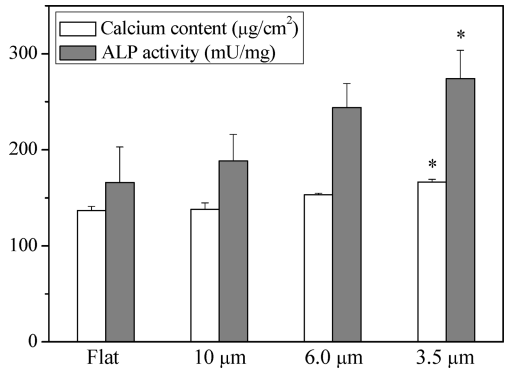

Figure 7. ALP activity and calcium content of MC3T3-E1 cells cultured on the flat and honeycomb films with different pore diameters for 14 days. *, $p < 0.05$ relative to the flat film.

ALP activity of MC3T3-E1 cells, two indicators of osteogenesis, on the honeycomb films were both higher than those on the flat one after 14 days of culture. These two parameters were even higher when the pores in the honeycomb films were smaller. These cell results were consistent with each other and indicated that honeycomb PCL films with 3.5 μm pores are potentially useful in bone regeneration and repair and this pore size can be fabricated into other biomaterials to promote adhesion, proliferation, and mineralization of bone cells.

To further analyze MC3T3-E1 cell differentiation, real-time PCR was used to assess mRNA expression of bone-specific differentiation markers. The results (Figure 8) demonstrated

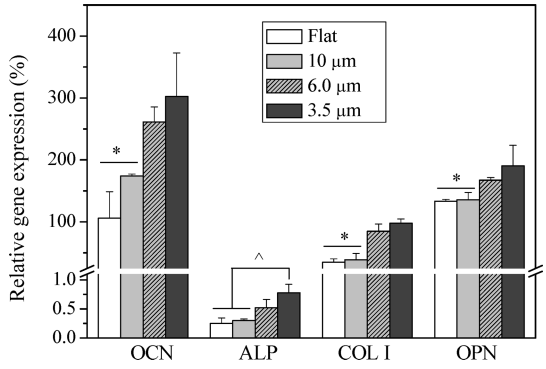

Figure 8. Gene expression levels of ALP, OCN, OPN, and COL I relative to GAPDH in MC3T3-E1 cells cultured for 14 days on the flat and honeycomb films with different pore diameters. *, $p < 0.05$ relative to others;^, $p < 0.05$.

that the expression levels of OCN, COL I, and OPN on the honeycomb films with pore diameters of 6.0 and 3.5 μm were significantly higher than those on the flat films and honeycomb films with 10 μm pores. For ALP, it had a significantly higher expression level on the honeycomb films with 3.5 μm pores than on other films. Cell and tissue development in bone formation have three stages: proliferation, matrix maturation, and mineralization, and different differentiation-related genes

reach their maximum expression levels at different stages.[43,55] The gene expression levels of ALP and COL I, which are early stage markers of osteogenesis, reach peak values in the stage of matrix maturation that occurs after 7 days of culture.[55] In contrast, OCN and OPN reach peak levels or continue to grow in the stage of mineralization.[43,55] Because the present results were obtained after 14 days of cell culture, which was in the mineralization stage, the relative expression levels of ALP and COL I were lower than those of OCN and OPN. The upregulated gene expression on the honeycomb films can be attributed to easier formation of integrin clusters and FAs, and better cell proliferation stimulated by the pore edges.

CONCLUSIONS

Honeycomb PCL films with different pore diameters have been fabricated using the breath-figure method in water-miscible THF without assistance of any surfactant. By increasing the airflow rate from 0 to 50 and 100 mL min^{-1}, uniform pores with controllable diameters from 10 to 6.0 and 3.5 μm were achieved, respectively. Compared with the flat control, the honeycomb films significantly promoted mouse MC3T3-E1 cell adhesion, spreading, proliferation, alkaline ALP activity, calcium content, and gene expression of bone-specific differentiation markers, ALP, COL I, OCN, and OPN, especially when the pores were smaller. The promotion originated from enhanced expression of integrin subunits of α_1, α_2, and β_1. Honeycomb PCL films could be stretched into groove-like structures. Compared with stretched flat films, stretched honeycomb films could elongate F-actin filaments of MC3T3-E1 cells significantly and the effect was more prominent when the pore diameter was smaller. These honeycomb PCL films can supply an efficient platform for bone tissue engineering applications.

AUTHOR INFORMATION

Corresponding Author

*E-mail: swang16@utk.edu. Tel: 1-865-974-7809. Fax: 1-865-974-4115.

Notes

The authors declare no competing financial interest.

ACKNOWLEDGMENTS

This work was supported by the start-up fund and professional development award from the University of Tennessee and Center for Materials Processing in the department.

REFERENCES

(1) Khan, Y.; Yaszemski, M. J.; Mikos, A. G.; Laurencin, C. T. *J. Bone Joint Surg. Am.* **2008**, *90A*, 36−42.
(2) Hing, K. A. *Philos. Trans. R. Soc. London, Ser. A* **2004**, *362*, 2821−2850.
(3) Bettinger, C. J.; Langer, R.; Borenstein, J. T. *Angew. Chem., Int. Ed.* **2009**, *48*, 5406−5415.
(4) Flemming, R. G.; Murphy, C. J.; Abrams, G. A.; Goodman, S. L.; Nealey, P. F. *Biomaterials* **1999**, *20*, 573−588.
(5) Harbers, G. M.; Grainger, D. W. In *Introduction to Biomaterials*; Guelcher, S. A., Hollinger, J. O., Eds.; CRC Press: Boca Raton, FL, 2005; pp 15−45.
(6) Anselme, K.; Bigerelle, M. *Int. Mater. Rev.* **2011**, *56*, 243−266.
(7) Dalby, M. J. *Med. Eng. Phys.* **2005**, *27*, 730−742.
(8) Tanaka, M. *Biochim. Biophys. Acta* **2011**, *1810*, 251−258.
(9) Bunz, U. H. F. *Adv. Mater.* **2006**, *18*, 973−989.
(10) Hernández-Guerrero, M.; Stenzel, M. H. *Polym. Chem* **2012**, *3*, 563−577.
(11) Woodruff, M. A.; Hutmacher, D. A. *Prog. Polym. Sci.* **2010**, *35*, 1217−1256.
(12) Tanaka, M.; Takebayashi, M.; Miyama, M.; Nishida, J.; Shimomura, M. *Bio-Med. Mater. Eng.* **2004**, *14*, 439−446.
(13) Formosa, F.; Sánchez-Vaquero, V.; Rodríguez-Navas, C.; Muñoz-Noval, Á.; Tejera-Sanchez, N.; Silván, M. M.; García-Ruiz, J. P.; Marletta, G. *Plasma Process. Polym.* **2010**, *7*, 794−801.
(14) Tsuruma, A.; Tanaka, M.; Yamamoto, S.; Shimomura, M. *Colloid. Surface. A* **2008**, *313*, 536−540.
(15) Yamamoto, S.; Tanaka, M.; Sunami, H.; Arai, K.; Takayama, A.; Yamashita, S.; Motita, Y.; Shimomura, M. *Surf. Sci.* **2006**, *600*, 3785−3791.
(16) McMillan, J. R.; Akiyama, M.; Tanaka, M.; Yamamoto, S.; Goto, M.; Abe, R.; Sawamura, D.; Shimomura, M.; Shimizu, H. *Tissue Eng.* **2007**, *13*, 789−798.
(17) Sunami, H.; Ito, E.; Tanaka, M.; Yamamoto, S.; Shimomura, M. *Colloids Surf., A* **2006**, *284*, 548−551.
(18) Tanaka, M.; Takayama, A.; Ito, E.; Sunami, H.; Yamamoto, S.; Shimomura, M. *J. Nanosci. Nanotechnol.* **2007**, *7*, 763−772.
(19) Arai, K.; Tanaka, M.; Yamamoto, S.; Shimomura, M. *Colloids Surf., A* **2008**, *313*, 530−535.
(20) Yamamoto, S.; Tanaka, M.; Sunami, H.; Ito, E.; Yamashita, S.; Morita, Y.; M. Shimomura, M. *Langmuir* **2007**, *23*, 8114−8120.
(21) Wang, B.; Mao, Z.; Meng, X.; Tong, W.; Gao, C. *Colloids Surf., B* **2010**, *76*, 38−43.
(22) Lee, S. J.; Choi, J. S.; Park, K. S.; Khang, G.; Lee, Y. M.; Lee, H. B. *Biomaterials* **2004**, *25*, 4699−4707.
(23) Orita, T.; Tomita, M.; Kato, K. *Colloids Surf., B* **2011**, *84*, 187−197.
(24) Zhao, B.; Zhang, J.; Wang, X.; Li, C. *J. Mater. Chem.* **2006**, *16*, 509−513.
(25) Park, M. S.; Kim, J. K. *Langmuir* **2004**, *20*, 5347−5352.
(26) Megelski, S.; Stephens, J. S.; Chase, D. B.; Rabolt, J. F. *Macromolecules* **2002**, *35*, 8456−8566.
(27) Casper, C. L.; Stephens, J. S.; Tassi, N. G.; Chase, D. B.; Rabolt, J. F. *Macromolecules* **2004**, *37*, 573−578.
(28) Wang, K.; Cai, L.; Hao, F.; Xu, X.; Cui, M.; Wang, S. *Biomacromolecules* **2010**, *11*, 2748−2759.
(29) Wang, K.; Cai, L.; Jesse, S.; Wang, S. *Langmuir* **2012**, *28*, 4382−4395.
(30) Wang, K.; Jesse, S.; Wang, S. *Macromol. Chem. Phys.* **2012**, *213*, 1239−1250.
(31) Cai, L.; Wang, S. *Polymer* **2010**, *51*, 164−177.
(32) Wang, K.; Cai, L.; Wang, S. *Polymer* **2011**, *52*, 2827−2839.
(33) Wang, K.; Cai, L.; Zhang, L.; Dong, J.; Wang, S. *Adv. Healthcare Mater* **2012**, *1*, 292−301.
(34) Cai, L.; Chen, J.; Rondinone, A. J.; Wang, S. *Adv. Func. Mater* **2012**, *22*, 3181−3190.
(35) Cassie, A. B. D.; Baxter, S. *Trans. Faraday Soc.* **1944**, *40*, 0546−0550.
(36) Murray, M. D.; Darvell, B. W. *J. Phys. D* **1990**, *23*, 1150−1155.
(37) Min, E. H.; Wong, K. H.; Stenzel, M. H. *Adv. Mater.* **2008**, *20*, 3550−3556.
(38) Biggs, M. J. P.; Dalby, M. J. *Proc. Inst. Mech. Eng., Part H* **2010**, *224*, 1441−1453.
(39) Geiger, B.; Spatz, J. P.; Bershadsky, A. D. *Nat. Rev.* **2009**, *10*, 21−33.
(40) Berry, C. C.; Campbell, G.; Spadiccino, A.; Robertson, M.; Curtis, A. S. G. *Biomaterials* **2004**, *25*, 5781−5788.
(41) Walboomers, X. F.; Croes, H. J. E.; Ginsel, L. A.; Jansen, J. A. *Biomaterials* **1998**, *19*, 1861−1868.
(42) Curtis, A.; Wilkinson, C. *Biomaterials* **1997**, *18*, 1573−1583.
(43) Siebers, M. C.; Brugge, P. J.; Walboomers, X. F.; Jansen, J. A. *Biomaterials* **2005**, *26*, 137−146.
(44) Anselme, K. *Biomaterials* **2000**, *21*, 667−681.
(45) Kim, E. J.; Boehm, C. A.; Mata, A.; Fleischman, A. J.; Muschler, G. F.; Roy, S. *Acta Biomater.* **2010**, *6*, 160−169.
(46) Park, J.; Bauer, S.; Schlegel, K. A.; Neukam, F. W.; von der Mark, K.; Schmuki, P. *Small* **2009**, *5*, 666−671.

(47) Park, J.; Bauer, S.; von der Mark, K.; Schmuki, P. *Nano Lett.* **2007**, *7*, 1686−1691.
(48) Thomas, C. H.; Collier, J. H.; Sfeir, C. S.; Healy, K. E. *Proc. Natl. Acad. Sci. U.S.A.* **2002**, *99*, 1972−1977.
(49) Davidson, P. M.; Özçelik, H.; Hasirci, V.; Reiter, G.; Anselme, K. *Adv. Mater.* **2009**, *21*, 3586−3590.
(50) Nishikawa, T.; Nonomura, M.; Arai, K.; Hayashi, J.; Sawadaishi, T.; Nishiura, Y.; Hara, M.; Shimomura, M. *Langmuir* **2003**, *19*, 6193−6201.
(51) Ingber, D. E. *J. Cell. Sci.* **1993**, *104*, 613−627.
(52) Maniotis, A. J.; Chen, C. S.; Ingber, D. E. *Proc. Natl. Acad. Sci. U.S.A.* **1997**, *94*, 849−854.
(53) Dalby, M. J.; Riehle, M. O.; Yarwood, S. J.; Wilkinson, C. D. W.; Curtis, A. S. G. *Exp. Cell Res.* **2003**, *284*, 274−282.
(54) Tan, P. S.; Teoh, S. H. *Mater. Sci. Eng., C* **2007**, *27*, 304−308.
(55) Stein, G. S.; Lian, J. B.; Owen., T. A. *FASEB J.* **1990**, *4*, 3111−3123.